Received: 9 November 2023 | Revised: 12 February 2024 | Accepted: 26 February 2024

DOI: 10.1111/cas.16151

Cancer Science WILEY

ORIGINAL ARTICLE

MFN2 suppresses the accumulation of lipid droplets and the progression of clear cell renal cell carcinoma

Zhiduan Cai[1] | Wenjun Luo[1] | Haoran Wang[1,2] | Rui Zhu[1] | Yaoji Yuan[1] | Xiangyu Zhan[1] | Mengyuan Xie[2] | Haoquan Zhuang[1] | Haoyu Chen[1] | Yuyu Xu[1] | Xiezhao Li[1] | Leyuan Liu[1] | Guibin Xu[1,3]

[1]Department of Urology, Key Laboratory of Biological Targeting Diagnosis, Therapy and Rehabilitation of Guangdong Higher Education Institutes, The Fifth Affiliated Hospital of Guangzhou Medical University, Guangzhou Medical University, Guangzhou, China

[2]Guangzhou Medical University, Guangzhou, China

[3]Guangdong Provincial Key Laboratory of Urology, The First Affiliated Hospital of Guangzhou Medical University, Guangzhou Medical University, Guangzhou, China

Correspondence
Guibin Xu, Department of Urology, The Fifth Affiliated Hospital of Guangzhou Medical University, Guangzhou Medical University, Guangzhou 510700, China.
Email: uro_xgb@163.com

Funding information
Guangzhou Key Laboratory of Biological Targeting Diagnosis and Therapy, Grant/Award Number: 202201020379; Characteristic Technology Project of Guangzhou Municipal Health Commission, Grant/Award Number: 2023C-TS50; Key Clinical Specialty Project of Guangdong Province, Grant/Award Number: 2022; Guangzhou Municipal Science and Technology Project, Grant/Award Number: 2024A03J0074; Key Laboratory of Guangdong Higher Education Institutes, Grant/Award Number: 2021KSYS009; Key Clinical Specialty Project of Guangzhou Medical University, Grant/Award Number: 2020; National Natural Science Foundation of China, Grant/Award Number: 81974392 and 82103359

Abstract

Dissolving the lipid droplets in tissue section with alcohol during a hematoxylin and eosin (H&E) stain causes the tumor cells to appear like clear soap bubbles under a microscope, which is a key pathological feature of clear cell renal cell carcinoma (ccRCC). Mitochondrial dynamics have been reported to be closely associated with lipid metabolism and tumor development. However, the relationship between mitochondrial dynamics and lipid metabolism reprogramming in ccRCC remains to be further explored. We conducted bioinformatics analysis to identify key genes regulating mitochondrial dynamics differentially expressed between tumor and normal tissues and immunohistochemistry and Western blot to confirm. After the target was identified, we created stable ccRCC cell lines to test the impact of the target gene on mitochondrial morphology, tumorigenesis in culture cells and xenograft models, and profiles of lipid metabolism. It was found that mitofusin 2 (MFN2) was downregulated in ccRCC tissues and associated with poor prognosis in patients with ccRCC. MFN2 suppressed mitochondrial fragmentation, proliferation, migration, and invasion of ccRCC cells and growth of xenograft tumors. Furthermore, MFN2 impacted lipid metabolism and reduced the accumulation of lipid droplets in ccRCC cells. MFN2 suppressed disease progression and improved prognosis for patients with ccRCC possibly by interrupting cellular lipid metabolism and reducing accumulation of lipid droplets.

KEYWORDS
clear cell renal cell carcinoma, Hif2α, lipid droplets, MFN2, mitochondrial fusion

Zhiduan Cai and Wenjun Luo contributed equally to this work.

1 | INTRODUCTION

Renal cell carcinoma is one of the most common malignant tumors in the urinary system. In 2023, renal cell carcinoma was among the top ten newly diagnosed cancers: the sixth among males and ninth among females in the United States.[1] Pathologically, 70%–75% of cases of renal cell carcinomas are clear cell renal cell carcinomas (ccRCC) that are characterized by the accumulation of lipid and glycogen within cytoplasm, often accompanied by reprogramming of glucose and fatty acid metabolism as well as tricarboxylic acid cycle.[2,3] Research has shown that levels of cholesterol esters, triglycerides, and cholesterol are significantly higher in ccRCC than in normal tissues.[4] Therefore, lipid metabolism reprogramming plays a crucial role in the progression of ccRCC, but its underlying mechanisms have not been fully elucidated.

Mitochondria are highly dynamic double-membrane-bound organelles in cells that maintain a dynamic balance of mitochondrial number and morphology through their fusion and fission.[5] This "mitochondrial dynamics" is closely involved in various cellular processes such as cell cycle, apoptosis, cell migration, mitochondrial autophagy, reactive oxygen species production, fatty acid oxidation, and lipid droplet formation.[6,7] Thus, mitochondrial dynamics has been shown to be associated with the initiation and development of different types of cancers including hepatocellular carcinoma, ovarian cancer, breast cancer, and pancreatic cancer.[6] For example, mitochondrial fission has been reported to promote cell migration, autophagy, tumor-associated macrophage infiltration, and the progression of hepatocellular carcinoma[8,9] and to trigger platinum resistance in ovarian cancer cells under hypoxic conditions.[10] Especially, blocking mitochondrial movement and fusion to form specialized subpopulations of mitochondria has been shown to enable single individual cell to be engaged in both fatty acid oxidation and lipid droplet formation, simultaneously.[7] Understanding the relationship between mitochondrial dynamics and accumulation of lipid droplets and their respective functions will provide new intervention targets for metabolic diseases such as ccRCC.

We initially conducted bioinformatics analysis of the mRNA data of ccRCC patients from two public databases to identify the differentially expressed genes between normal and tumor tissues which were common among the two databases. We specifically identified mitofusin 2 (MFN2) as the only mitochondrial dynamics-related gene that was significantly downregulated in ccRCC tissues and associated with poor prognosis for ccRCC patients. MFN2, originally named as hyperplasia suppressor gene (HSG), was renamed because of its role in controlling mitochondrial fusion.[11] MFN2 in addition to MFN1 was also found to regulate phospholipid and cholesterol synthesis in type II alveolar epithelial cells of the lung, and the deletion of MFN1 and MFN2 led to block lipid synthesis by inducing defects of fatty acid synthetase (FAS) and exacerbate bleomycin-induced pulmonary fibrosis.[12] Interestingly, MFN2 directly interacts with perilipin, an outer shell protein of lipid droplets, promoting interaction between mitochondria and lipid droplets and influencing lipid metabolism processes and systemic energy balance in brown adipose tissue.[13] It was recently revealed that MFN2 inhibits the progression of ccRCC by regulating EGFR-dependent mitochondrial dephosphorylation.[14] In our study, we confirmed the role of MFN2 as a suppressor gene of ccRCC and found that MFN2 in ccRCC tissues may act as a suppressor to reduce the accumulation of lipid droplets and the development of ccRCC.

2 | MATERIALS AND METHODS

2.1 | Bioinformatics analysis

The clinical and RNA-seq data deposited in The Cancer Genome Atlas Kidney Renal Clear Cell Carcinoma (TCGA-KIRC) were downloaded from the public TCGA database (https://portal.gdc.cancer.gov). The mRNA expression data-set of ccRCC tumors and adjacent nontumor renal tissues GSE40435 were downloaded from the Gene Expression Omnibus (GEO) database. Detailed information on R packages is the same as described previously.[14]

2.2 | Collecting renal tissues from patients

In order to examine the expression levels of MFN2 protein by immunohistochemistry (IHC), we purchased a tissue microarray (TMA) KD1504 containing kidney tumor and adjacent normal renal tissues from 50 ccRCC patients from Xi'an Alina, China. To measure the levels of MFN2 protein by Western blot (WB), we collected 14 pairs of tumor and adjacent normal tissues from patients diagnosed with ccRCC at the Fifth Affiliated Hospital of Guangzhou Medical University.

2.3 | Culturing and establishing stable lines of renal cells

The immortalized renal epithelial cell line HK-2 and ccRCC cell lines 769-P, 786-O, and Caki-1 were obtained from the Cell Bank/Stem Cell Bank of the Chinese Academy of Sciences Typical Culture Preservation Committee. MFN2 shRNA, control lentiviruses, and Hif2α siRNA were purchased from Shanghai Jikai Gene Company. The sequence was as follows: sh-MFN2-1 gcAGGTTTACTGCGAGGAAAT; sh-MFN2-2 gtCAAAGGTTACCTATCCAAA; si-Hif2α-1 AGGTGGAGCTAACAGGACATA; si-Hif2α-2 CGACCTGAAGATTGAAG TGAT. HitransG (Jikai) was used to facilitate efficient viral infection of cells. Screening was conducted 3 days after treatment with puromycin (MA0318, Meilun).

2.4 | Analyzing protein levels by IHC and WB

Immunohistochemistry or WB was used to detect the protein expression levels of tissues or cells according to the protocols we

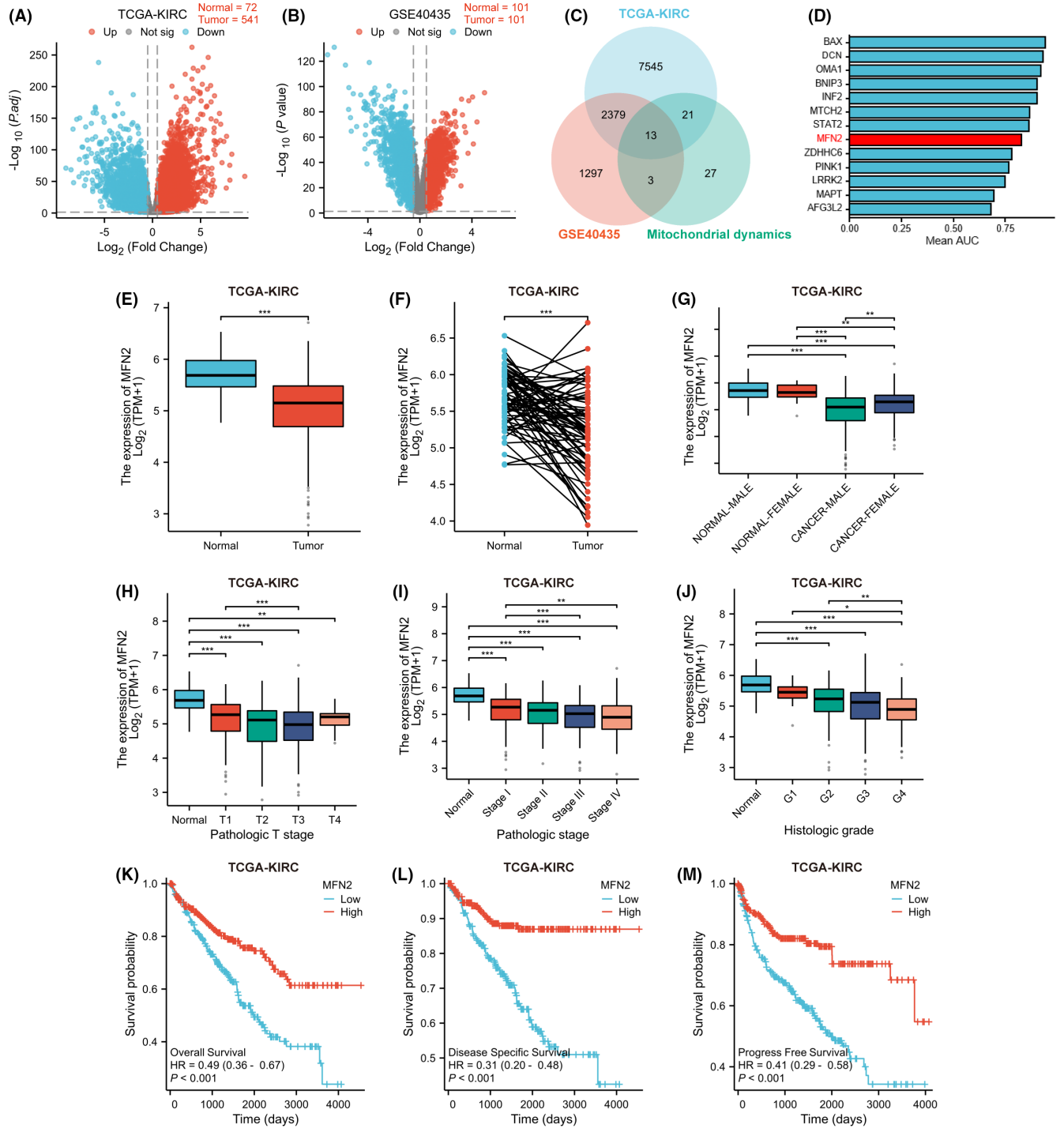

FIGURE 1 A reduced expression of MFN2 mRNA was detected in human clear cell renal cell carcinoma (ccRCC) tissues deposited in databases and predicted a poor prognosis. (A, B) Volcano plots of differentially expressed genes between tumor and normal tissues deposited in The Cancer Genome Atlas Kidney Renal Clear Cell Carcinoma (TCGA-KIRC) (A) and GSE40435 database (B). (C) Venn diagram showing the number of differentially expressed genes in ccRCC tumorigenesis between and among those from TCGA-KIRC, GSE40435 database, and a GO mitochondrial morphology gene set. (D) An AUC plot showing the prognostic values of the 13 differentially expressed mitochondrial dynamics-regulating genes as identified above (C) based on the TCGA-KIRC database. (E–J) Plots showing differences of expression levels of MFN2 mRNA between 541 tumor and 72 adjacent normal tissues (E), 72 pairs of tumor and adjacent normal tissues (F), different genders (G), different T stages based on the classification reported in AJCC 8th edition (H), different clinical stages (I), and pathological grade (J) deposited in the TCGA-KIRC database. (K–M) Kaplan–Meier curves showing the overall survival (K), disease-free survival (L), and progression-free survival (M) for ccRCC patients with high or low expression levels of MFN2 based on a median cutoff in the TCGA-KIRC cohort. $^{*}p < 0.05$, $^{**}p < 0.01$, $^{***}p < 0.001$.

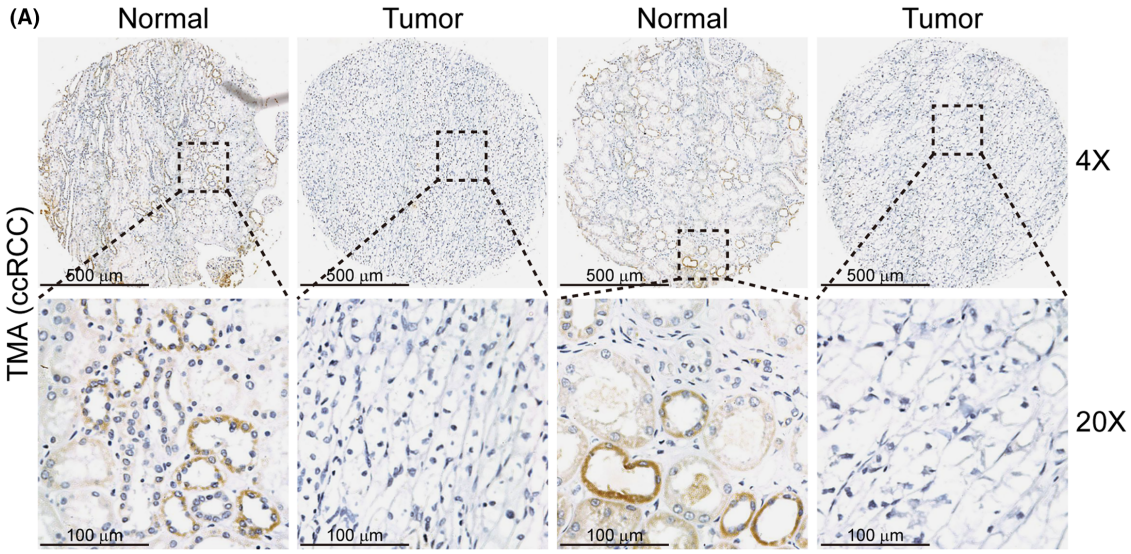
(A)
Normal
Tumor
Normal
Tumor
TMA (ccRCC)
4X
20X
500 μm
100 μm

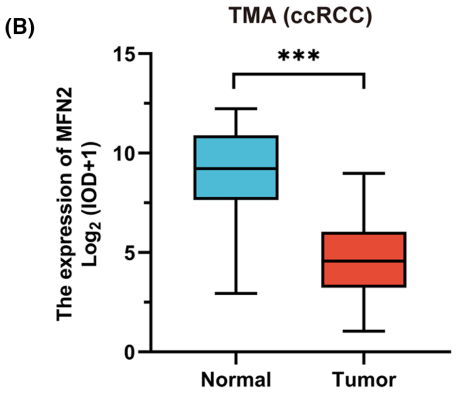
(B)
TMA (ccRCC)
***
The expression of MFN2
Log2 (IOD+1)
15
10
5
0
Normal
Tumor

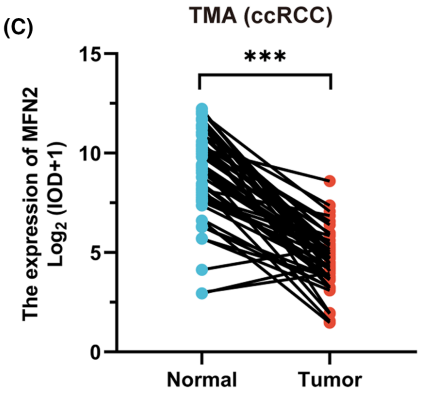
(C)
TMA (ccRCC)
***
The expression of MFN2
Log2 (IOD+1)
15
10
5
0
Normal
Tumor

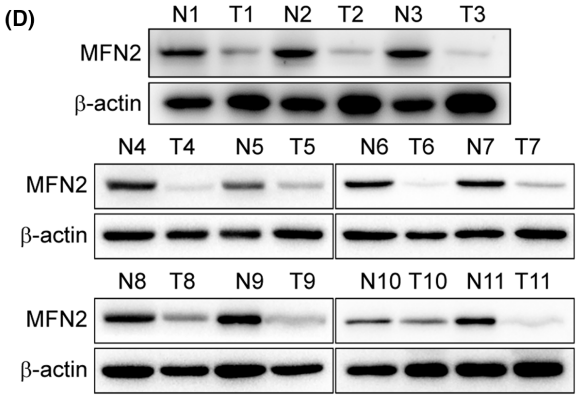
(D)
N1 T1 N2 T2 N3 T3
MFN2
β-actin
N4 T4 N5 T5 N6 T6 N7 T7
MFN2
β-actin
N8 T8 N9 T9 N10 T10 N11 T11
MFN2
β-actin

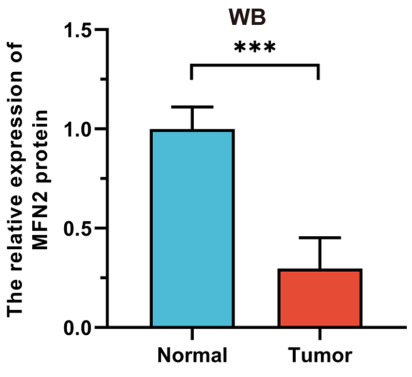
WB
***
The relative expression of
MFN2 protein
1.5
1.0
0.5
0.0
Normal
Tumor

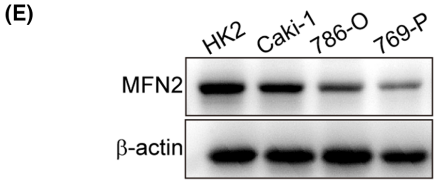
(E)
HK2
Caki-1
786-O
769-P
MFN2
β-actin

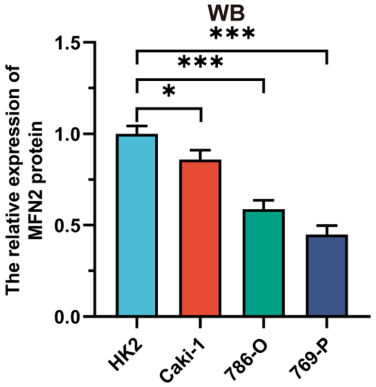
WB
***
***
*
The relative expression of
MFN2 protein
1.5
1.0
0.5
0.0
HK2
Caki-1
786-O
769-P

FIGURE 2 A reduced expression of the MFN2 protein was similarly confirmed with clinical samples from human clear cell renal cell carcinoma (ccRCC) patients. (A–C) Representative images (A) and quantitative analyses (B, C) showing the differences of MFN2 protein levels as detected by immunohistochemistry (IHC) staining between all tumor and normal tissues (B) and between the 50 pairs of tumor and adjacent normal tissues (C) collected in a human ccRCC tissue microarray (TMA) (A). (D) Representative images and a quantitative plot showing the differences of MFN2 protein levels as detected by Western blot (WB) between tumor and adjacent normal tissues from 11 human ccRCC patients enrolled in our hospital. (E) Representative images and quantitative analysis showing the MFN2 protein levels as detected by WB in immortalized renal epithelial cell line HK-2 and ccRCC cell lines Caki-1, 786-O, and 769-P. β-Actin protein was used as a loading control. $^{*}p<0.05$, $^{***}p<0.001$.

previously reported.[15,16] Specific primary antibodies were shown in Appendix S1. IHC images were captured using a scanner model Pannoramic MIDI and Case Viewer software (3DHISTECH Ltd.) and quantitatively analyzed for integrated optical density (IOD) using Image-Pro Plus software (6.0, Media Cybernetics). The ChemiDoc™ XRS system and Image Lab software (3.0, Bio-Rad) were used to capture luminescent results in WB.

2.5 | Visualizing mitochondria

The ccRCC cells were seeded on a confocal dish (BS-20-GJM, Biosharp), cultured for 24 h, starved for 12 h using EBSS (24010043, Gbico), and stained with MitoTracker Orange (100 nM, M7510, Thermo) and Hoechst 33342 (10 mg/mL, MA0126, Meilun) for 30 min. The images were captured using a confocal microscope (ZEISS), and the lengths of mitochondrial branches were quantified with the Image J software (1.54, NIH). To observe mitochondria in frozen tissues, ccRCC and adjacent normal tissues collected from patients enrolled in our hospital were sent to KingMed Diagnosis to prepare tissue sections for us to observe mitochondria with transmission electron microscope.

2.6 | Measuring the rates of cell proliferation, migration, and invasion

To measure the rates of cell proliferation, the corresponding ccRCC cells were tested with CCK8 (MA0218, Meilun). To measure rates of cell migration, ccRCC cells were seeded in culture-insert 2 wells (80209, ibidi). Transwell assays (3422, 8 μm pore size, Corning Inc.) were also applied to assess the rates of migration and invasion of ccRCC cells. Detailed experimental procedures were the same as described previously.[15,16]

2.7 | Testing the impact of MFN2 on tumorigenesis in animal model

To test the impact of MFN2 on tumorigenesis, the respective ccRCC cells were collected and mixed with Matrigel (354248, Corning Inc.) to 5,000,000 cells/100 μL. Then, 100 μL cells were injected into the axilla of 4-week-old nude mice (Bai Shi Tong Biotechnology Co., Ltd.). Tumor volumes were calculated using the formula $V=$ long diameter $\times$ short diameter^2 $\times 0.5$. The tumors were collected at 45 days after cell injection, their morphology was captured with a digital camera, and weights were recorded.

2.8 | Analyzing lipid metabolomics

Cells were collected for lipid metabolomics analysis using the liquid chromatography tandem mass spectrometry (LC-MS) of APExBIO company. The identification of metabolites was based on accurate mass and secondary fragments by searching the Lipidmaps database (http://www.lipidmaps.org/). The levels of lipid metabolites were quantitatively determined based on a standard curve calibration.

2.9 | Observing lipid droplets by oil red O staining

To observe lipid droplets accumulated in cells, ccRCC cells were inoculated on a slide (WHB-6-CS, WHB) in a six-well plate, cultured for 24 h, fixed with 4% paraformaldehyde (MA0192, Meilun) for 15 min, and stained according to the instructions associated with the oil red O staining kit (DL0008, Leagene). The staining of oil red O was observed under the microscope, and the IOD was obtained by Image-Pro Plus software for quantitative analysis.

2.10 | Statistical analysis

All experiments were repeated at least three times and the results are presented as mean ± standard deviation. All statistical analyses were performed using the GraphPad Prism software version 9.0 (USA). Statistical significance was set at $p<0.05$. The statistical significance of quantitative data was analyzed by Student's *t*-test or analysis of variance (ANOVA). The Kaplan–Meier method and log-rank test were used for survival analysis.

3 | RESULTS

3.1 | MFN2 was similarly identified as a favorable prognostic marker for ccRCC patients

In order to screen for key regulatory factors in ccRCC tumor progression, we analyzed the differentially expressed genes between cancerous and normal tissues from the ccRCC cohorts in both TCGA

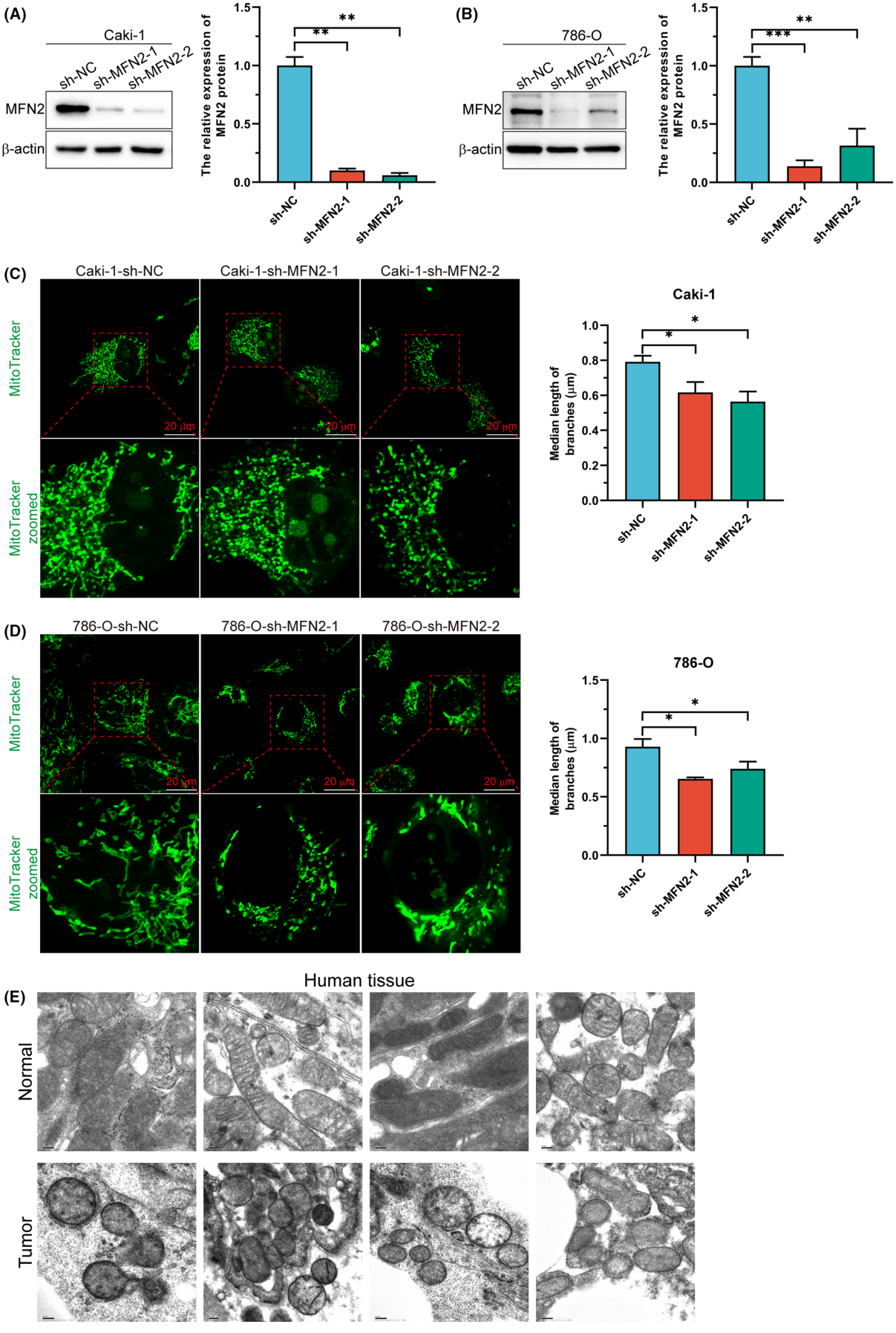
(A)
Caki-1
sh-NC
sh-MFN2-1
sh-MFN2-2
MFN2
β-actin
The relative expression of MFN2 protein
(B)
786-O
(C)
Caki-1-sh-NC
Caki-1-sh-MFN2-1
Caki-1-sh-MFN2-2
MitoTracker
MitoTracker zoomed
20 μm
Caki-1
Median length of branches (μm)
(D)
786-O-sh-NC
786-O-sh-MFN2-1
786-O-sh-MFN2-2
786-O
(E)
Human tissue
Normal
Tumor

FIGURE 3 Suppressing the expression of MFN2 led to mitochondrial fragmentation in clear cell renal cell carcinoma (ccRCC) cells. (A, B) Representative images and quantitative analysis showing MFN2 protein levels as detected by Western blot (WB) in Caki-1 (A) and 786-O cells (B) transfected with two MFN2-specific shRNA (sh-MFN2-1 and sh-MFN2-2) or a negative control virus (sh-NC). (C, D) Representative images and quantitative plots showing the sizes of mitochondria labeled with MitoTracker (green color) in Caki-1 (C) and 786-O cells (D) transfected with sh-MFN2-1 and sh-MFN2-2 or a sh-NC virus. (E) Representative images showing the morphology of mitochondria in tumor and adjacent normal tissues. $^{*}p<0.05$, $^{**}p<0.01$, $^{***}p<0.001$.

and GSE40435 public databases. We found 9958 genes differentially expressed between normal and ccRCC tissues deposited in the TCGA-KIRC database and 3692 genes differentially expressed between normal and ccRCC tissues deposited in the GSE40435 database (Figure 1A,B). Mitochondrial dynamics are closely related to the initiation and development of human cancers.[6] Moreover, the progression of ccRCC is accompanied with metabolic reprogramming, which is closely related to mitochondrial function.[3] Thus, we compared the differentially expressed genes identified from the two databases described above with a GO mitochondrial morphology gene set and found 13 mitochondrial dynamics-regulating genes which were differentially expressed between normal and ccRCC tissues in both databases: Six genes were overexpressed and seven genes were suppressed in human ccRCC tissues (Figure 1C,D). Based on the prognostic information from the TCGA-KIRC database, we calculated the area under the curve (AUC) values of the 13 genes and found all 13 genes were good predictors of ccRCC patients' prognosis (Figure 1D). Among these genes, MFN2 was the only one gene that was significantly downregulated in ccRCC tumor tissues (Figure 1E,F) and also directly involved in mitochondrial fusion regulation. MFN2 was also significantly downregulated in ccRCC tumor tissues in the GSE40435 database (Figure S1A,B). During the preparation of the manuscript, similar results were independently reported with the same TCGA-KIRC database but a different dataset GSE73121 showing the differences between primary tumors and metastatic tumors.[14] Although it has been reported as a tumor suppressor gene in various tumors[17,18] including ccRCC,[14] its specific mechanism of action remains unclear. MFN2 has also been reported to be involved in lipid metabolism.[12] As lipid metabolic reprogramming is a key feature of ccRCC progression,[3] we chose to continue investigating the relationship between MFN2 and lipid metabolism in ccRCC.

Further analyzing the information from the TCGA-KIRC database, we found that expression levels of MFN2 were significantly lower in ccRCC tissues from male than from female patients although they were not significantly different between the normal tissues from male and female patients (Figure 1G). A trend of decreasing expression levels of MFN2 was found to be associated with increasing T stages (Figure 1H), clinical stage (Figure 1I), and histological grade (Figure 1J). However, the expression levels of MFN2 exhibited no significant difference between male and female patients in both normal and tumor tissues and among different grades of patients in tumor tissues in the GSE40435 database (Figure S1C,D). To further assess the prognostic value of MFN2 for ccRCC patients, we analyzed the survival data deposited in the TCGA-KIRC database and found that higher expression levels of MFN2 were associated with better overall survivals, disease-specific survivals, and progression-free survivals for ccRCC patients (Figure 1K–M). Overall, these findings suggest that MFN2 is a favorable prognostic indicator for ccRCC patients.

3.2 | A reduced expression of MFN2 in ccRCC was similarly confirmed at protein level

Reduced levels of MFN2 mRNA described above suggested a potential but not a certainty that levels of MFN2 protein were reduced in ccRCC tissues. To confirm, we conducted IHC with a commercially available ccRCC tumor TMA and found that levels of MFN2 protein were significantly reduced in tumor tissues based on not only a comparison of all tumor tissues with all normal tissues but also a comparison of the tumor tissues with their respective adjacent normal tissues (Figure 2A–C). The expression levels of MFN2 exhibited no significant difference among different age groups, T stages, or histological grades (Table S1). Further analyses with 11 pairs of tumor and adjacent normal tissues from ccRCC patients enrolled in our hospital with WB revealed that levels of MFN2 protein in tumor tissues were significantly lower than those in adjacent normal tissues (Figure 2D). Subsequently, we examined the expression levels of MFN2 in human ccRCC cells (786-O, 769-P, and Caki-1) and noncancerous immortalized renal epithelial HK-2 cells and similarly found that the expression levels of MFN2 protein were lower in tumor cells than in normal cells (Figure 2E). Here again, we independently confirm with more samples that expression levels of MFN2 protein are similarly reduced in ccRCC tissues.[14]

3.3 | MFN2 promoted mitochondrial fusion

In order to explore the potential role of MFN2 in the development of ccRCC, we used the Caki-1 and 786-O cells with high levels of MFN2 protein and successfully created two sets of stable cell lines, among which one expressed normal levels and two expressed significantly reduced levels of MFN2 protein (Figure 3A,B). Since MFN2 has been identified as an important protein that promotes mitochondrial fusion,[11,19] we stained cells with a green fluorescence dye MitoTracker to label mitochondria and found that cells with suppressed levels of MFN2 had significantly shorter mitochondrial fragments (Figure 3C,D). Since levels of MFN2 were reduced in ccRCC tissues (Figure 1), we examined the mitochondria in renal tissues from patients enrolled in our hospital with transmission electron microscope and found an intensive mitochondrial fragmentation was associated with reduced levels of MFN2 in ccRCC tissues (Figure 3E). Therefore,

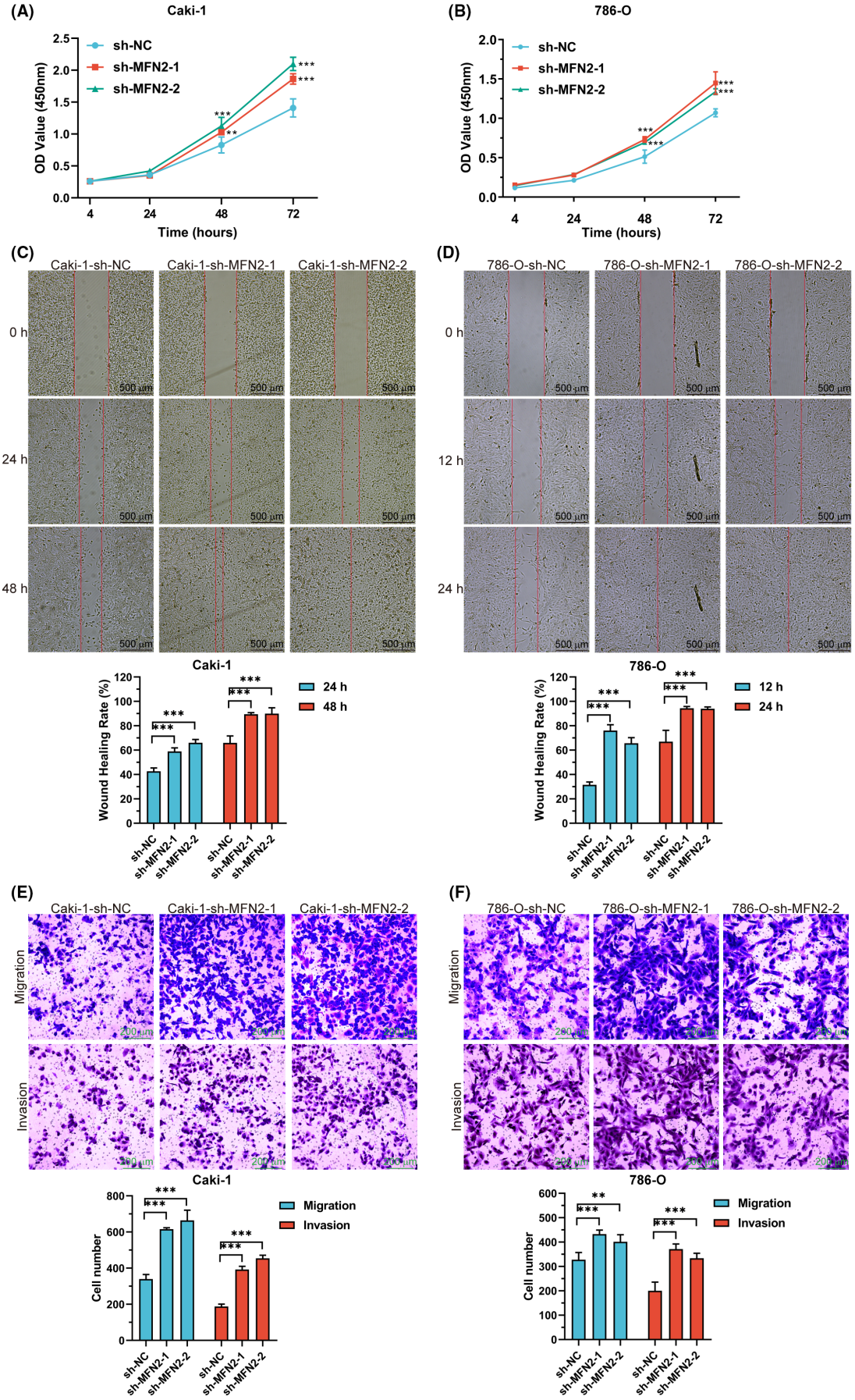
(A)
Caki-1
sh-NC
sh-MFN2-1
sh-MFN2-2
OD Value (450nm)
Time (hours)
(B)
786-O
(C)
Caki-1-sh-NC
Caki-1-sh-MFN2-1
Caki-1-sh-MFN2-2
0 h
24 h
48 h
500 μm
Caki-1
Wound Healing Rate (%)
24 h
48 h
(D)
786-O-sh-NC
786-O-sh-MFN2-1
786-O-sh-MFN2-2
0 h
12 h
24 h
786-O
12 h
24 h
(E)
Migration
Invasion
Caki-1
Cell number
Migration
Invasion
(F)
786-O

FIGURE 4 Suppressing the expression of MFN2 led to enhancements of proliferation, migration, and invasion of clear cell renal cell carcinoma (ccRCC) cells. (A, B) Plots showing the growth curves based on CCK-8 assays in Caki-1 (A) and 786-O cells (B) transfected with sh-MFN2-1 and sh-MFN2-2 or a sh-NC virus. (C–F) Representative images (top) and statistical analysis (bottom) showing the scratch-healing experimental results (C, D) and migration and invasion experimental results (E, F) of Caki-1 (C, E) and 786-O cells (D, F) transfected with sh-MFN2-1 and sh-MFN2-2 or a sh-NC virus. $^{**}p < 0.01$, $^{***}p < 0.001$.

MFN2 in ccRCC cells plays the same role to promote mitochondrial fusion as expected.

3.4 | MFN2 suppressed the proliferation, migration, and invasion of ccRCC cells

To test the impact of MFN2 on the progression and malignancy of ccRCC cells, we conducted CCK-8 assays and found that cells with reduced levels of MFN2 had significantly higher rates of proliferation (Figure 4A,B). Results from cell scratch assays revealed that cells with MFN2 suppressed had significantly higher rates of lateral migration (Figure 4C,D). Results from transwell assays indicated that cells with reduced levels of MFN2 displayed significantly higher rates of vertical migration and invasion (Figure 4E,F). These findings suggest that MFN2 suppresses the progression of ccRCC.

3.5 | MFN2 suppressed the growth of ccRCC tumors

In order to explore the impact of MFN2 on tumorigenesis, we used two pairs of established cell lines including one MFN2-knockout ccRCC cell line with sh-MEN2-1 and the corresponding control cell line with sh-NC to create xenograft tumor models in which tumor cells were injected subcutaneously into nude mice. We collected the tumor tissues 45 days after cell injection and found that MFN2-knockdown cells developed larger tumors with both larger tumor volume and more tumor weight than the control cells (Figure 5A,B), which is consistent with the results that overexpression of MFN2 leads to decreases in tumor volume and weight.[14] IHC analyses of tumor tissue sections revealed that suppressing the expression of MFN2 resulted in significant increases in levels of proteins Ki-67 and PCNA (Figure 5C,D), two well-established proliferation markers for tumor cells.[20,21] Therefore, MFN2 suppresses the growth of ccRCC tumors.

3.6 | MFN2 suppressed the accumulation of lipid droplets in ccRCC cells

The accumulation of lipid droplets, leading to the appearance of clear cells after H&E staining, is one of the most predominant characteristics of ccRCC.[22,23] We performed LC-MS analysis to detect the changes of lipid metabolites in cells after MFN2 was suppressed. Hierarchical clustering heatmaps showed that levels of 20 lipid metabolites were detected to be significantly changed in both cells and levels of 13 were increased and 7 reduced in cells when MFN2 was suppressed (Figure 6A,B). The 13 lipid metabolites with increased levels included six triglyceride metabolites, which are the fat circulating in blood[24]: TG(16:0/20:1(11Z)/20:2(11Z,14Z))[iso6], TG(21:0/22:3(10Z,13Z,16Z)/22:4(7Z,10Z,13Z,16Z))[iso6], TG(20:5(5Z,8Z,11Z,14Z,17Z)/21:0/22:0)[iso6], TG(20:1(11Z)/20:3(8Z,11Z,14Z)/22:3(10Z,13Z,16Z))[iso6], TG(19:1(9Z)/19:1(9Z)/20:1(11Z))[iso3], and TG(19:0/12:0/19:0) (d5); 3 membrane-associated phosphatidylcholine metabolites promoting cancer malignant growth[25]: PC(22:4(7Z,10Z,13Z,16Z)/22:1(11Z)), PC(20:5(5Z,8Z,11Z,14Z,17Z)/18:3(9Z,12Z, 15Z)), and PC(22:6(4Z,7Z,10Z,13Z,16Z,19Z)/20:3(8Z,11Z,14Z)); 3 membrane-associated sphingolipids: C17 Sphinganine, Cer(d18:0/16:0), and Clavepictine B; and a diradylglycerol 1-(8-[3]-ladderane-octanoyl-2-(8-[3]-ladderane-octanyl)-sn-glycerol). The seven with decreased levels included three sphingolipids: KDNalpha2-3Galbeta1-4(Fucalpha1-3)GlcNAcbeta1-3Galbeta1-4Glcbeta-Cer(d18:1/26:0), NeuAcalpha2-6Galbeta1-3GalNAcbeta1-3Galalpha1-4Galbeta1-4Glcbeta-Cer(d18:1/22:0), and NeuGcalpha2-8NeuGcalpha2-3Galbeta1-3GalNAcbeta1-3Galalpha1-4Galbeta1-4Glcbeta-Cer(d18:1/16:0); bile acid ursodeoxycholic acid; vitamin D 1alpha-hydroxy-23-[3-(1-hydroxy-1-methylethyl) phenyl]-22,22,23,23-tetradehydro-24,25,26,27-tetranorvitamin D3/1alpha-hydroxy-23-[3-(1-hydroxy-1-methylethyl) phenyl]-22,22,23,23-tetradehydro-24,25,26,27-tetranorcholecalciferol; phosphatidylserine PS(P-18:0/12:0); and 18:1 cholesteryl ester (d5) (Figure 6C,D). We further performed oil red O staining to assess lipid distribution within ccRCC cells and found that MFN2-knockdown cells accumulated more lipid droplets (Figure 6E,F). In general, these results suggest that MFN2 suppresses the accumulation of lipid droplets in ccRCC cells.

3.7 | MFN2 suppressed the expression of proteins involved in lipid metabolism in ccRCC cells

The accumulation of lipid droplets in cells is potentially the consequence of increasing synthesis and/or decreasing degradation of lipid droplets.[26] We analyzed the levels of proteins related to lipogenesis and found that acetyl-CoA synthetase 1 (AceCS1), acetyl-CoA synthetase long-chain family member 1 (ACSL1), acetyl-CoA carboxylase (ACC), and FAS, four key proteins involved in fatty acid and lipid synthesis,[27–31] were significantly increased in cells whose expression levels of MFN2 were suppressed (Figure 7A,B). Meanwhile, we also detected an increase in the expression levels of perilipin2 protein in cells with MFN2 suppressed (Figure 7C,D), indicating the lipid droplets were better protected from being degraded through lipophagy.[32]

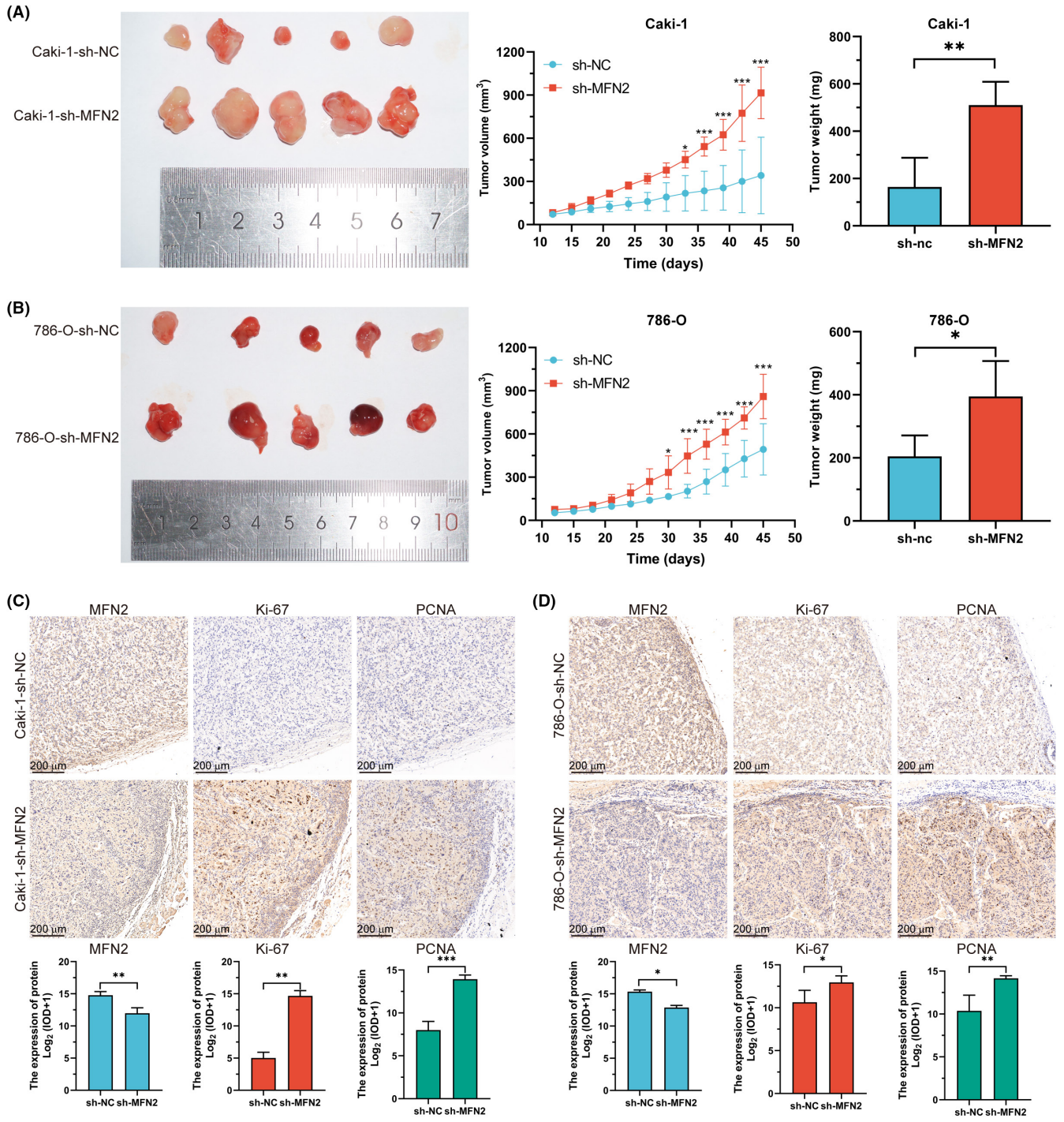

FIGURE 5 Suppressing the expression of MFN2 led to an acceleration of clear cell renal cell carcinoma (ccRCC) tumor growth in xenograft mouse models. (A, B) Representative images and plots showing the morphology and respective volumes and weights of subcutaneous tumors formed from Caki-1 (A) and 786-O (B) cells transfected with the mixture of sh-MFN2-1 and sh-MFN2-2 or a sh-NC virus. (C, D) Representative images and quantitative analyses showing the expression levels of MFN2, Ki-67, and PCNA proteins as detected by immunohistochemistry (IHC) staining in tumors formed from Caki-1 (C) and 786-O (D) transfected with the mixture of sh-MFN2-1 and sh-MFN2-2 or a sh-NC virus. $^{*}p < 0.05$, $^{**}p < 0.01$, $^{***}p < 0.001$.

FIGURE 6 Suppressing the expression of MFN2 caused a disruption of lipid metabolism in clear cell renal cell carcinoma (ccRCC) cells. (A, B) Heatmaps showing differentially changed levels of lipid metabolites in Caki-1 (A) and 786-O (B) cells transfected with the mixture of sh-MFN2-1 and sh-MFN2-2 or a sh-NC virus. (C, D) Plots showing the relative levels of lipid metabolites in Caki-1 (C) and 786-O (D) cells transfected with the mixture of sh-MFN2-1 and sh-MFN2-2 or a sh-NC virus. (E, F) Representative images of oil red O staining and quantitative plots of integrated optical density (IOD) in Caki-1 (D) and 786-O (E) cells transfected with sh-MFN2-1, sh-MFN2-2, or a sh-NC virus. $^{*}p < 0.05$, $^{**}p < 0.01$, $^{***}p < 0.001$.

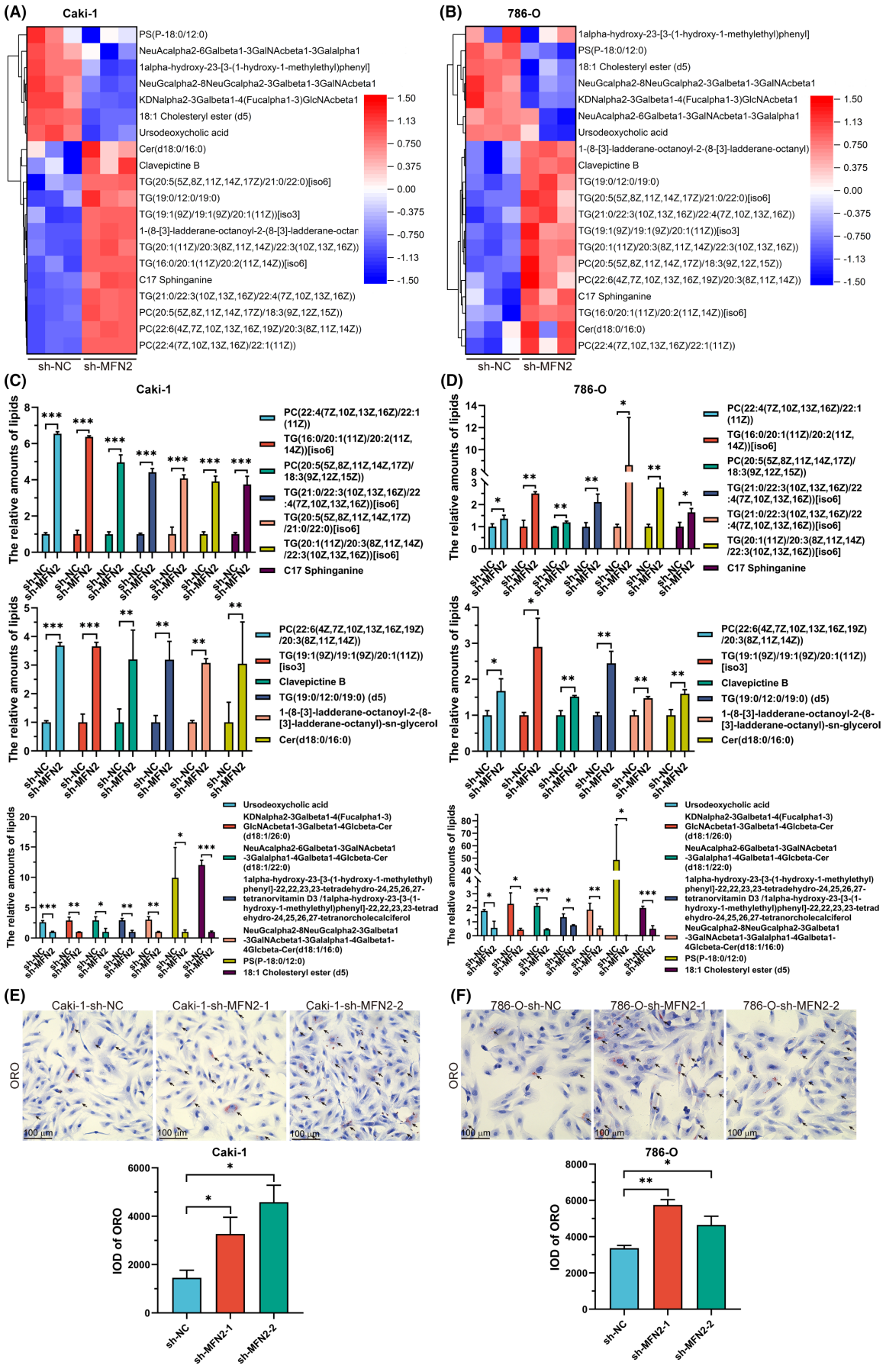
(A)
Caki-1
PS(P-18:0/12:0)
NeuAcalpha2-6Galbeta1-3GalNAcbeta1-3Galalpha1
1alpha-hydroxy-23-[3-(1-hydroxy-1-methylethyl)phenyl]
NeuGcalpha2-8NeuGcalpha2-3Galbeta1-3GalNAcbeta1
KDNalpha2-3Galbeta1-4(Fucalpha1-3)GlcNAcbeta1
18:1 Cholesteryl ester (d5)
Ursodeoxycholic acid
Cer(d18:0/16:0)
Clavepictine B
TG(20:5(5Z,8Z,11Z,14Z,17Z)/21:0/22:0)[iso6]
TG(19:0/12:0/19:0)
TG(19:1(9Z)/19:1(9Z)/20:1(11Z))[iso3]
1-(8-[3]-ladderane-octanoyl-2-(8-[3]-ladderane-octar
TG(20:1(11Z)/20:3(8Z,11Z,14Z)/22:3(10Z,13Z,16Z))
TG(16:0/20:1(11Z)/20:2(11Z,14Z))[iso6]
C17 Sphinganine
TG(21:0/22:3(10Z,13Z,16Z)/22:4(7Z,10Z,13Z,16Z))
PC(20:5(5Z,8Z,11Z,14Z,17Z)/18:3(9Z,12Z,15Z))
PC(22:6(4Z,7Z,10Z,13Z,16Z,19Z)/20:3(8Z,11Z,14Z))
PC(22:4(7Z,10Z,13Z,16Z)/22:1(11Z))
1.50
1.13
0.750
0.375
0.00
-0.375
-0.750
-1.13
-1.50
sh-NC
sh-MFN2
(B)
786-O
1alpha-hydroxy-23-[3-(1-hydroxy-1-methylethyl)phenyl]
PS(P-18:0/12:0)
18:1 Cholesteryl ester (d5)
NeuGcalpha2-8NeuGcalpha2-3Galbeta1-3GalNAcbeta1
KDNalpha2-3Galbeta1-4(Fucalpha1-3)GlcNAcbeta1
NeuAcalpha2-6Galbeta1-3GalNAcbeta1-3Galalpha1
Ursodeoxycholic acid
1-(8-[3]-ladderane-octanoyl-2-(8-[3]-ladderane-octanyl)
Clavepictine B
TG(19:0/12:0/19:0)
TG(20:5(5Z,8Z,11Z,14Z,17Z)/21:0/22:0)[iso6]
TG(21:0/22:3(10Z,13Z,16Z)/22:4(7Z,10Z,13Z,16Z))
TG(19:1(9Z)/19:1(9Z)/20:1(11Z))[iso3]
TG(20:1(11Z)/20:3(8Z,11Z,14Z)/22:3(10Z,13Z,16Z))
PC(20:5(5Z,8Z,11Z,14Z,17Z)/18:3(9Z,12Z,15Z))
PC(22:6(4Z,7Z,10Z,13Z,16Z,19Z)/20:3(8Z,11Z,14Z))
C17 Sphinganine
TG(16:0/20:1(11Z)/20:2(11Z,14Z))[iso6]
Cer(d18:0/16:0)
PC(22:4(7Z,10Z,13Z,16Z)/22:1(11Z))
1.50
1.13
0.750
0.375
0.00
-0.375
-0.750
-1.13
-1.50
sh-NC
sh-MFN2
(C)
Caki-1
The relative amounts of lipids
PC(22:4(7Z,10Z,13Z,16Z)/22:1(11Z))
TG(16:0/20:1(11Z)/20:2(11Z,14Z))[iso6]
PC(20:5(5Z,8Z,11Z,14Z,17Z)/18:3(9Z,12Z,15Z))
TG(21:0/22:3(10Z,13Z,16Z)/22:4(7Z,10Z,13Z,16Z))[iso6]
TG(20:5(5Z,8Z,11Z,14Z,17Z)/21:0/22:0)[iso6]
TG(20:1(11Z)/20:3(8Z,11Z,14Z)/22:3(10Z,13Z,16Z))[iso6]
C17 Sphinganine
PC(22:6(4Z,7Z,10Z,13Z,16Z,19Z)/20:3(8Z,11Z,14Z))
TG(19:1(9Z)/19:1(9Z)/20:1(11Z))[iso3]
Clavepictine B
TG(19:0/12:0/19:0) (d5)
1-(8-[3]-ladderane-octanoyl-2-(8-[3]-ladderane-octanyl)-sn-glycerol
Cer(d18:0/16:0)
Ursodeoxycholic acid
KDNalpha2-3Galbeta1-4(Fucalpha1-3)GlcNAcbeta1-3Galbeta1-4Glcbeta-Cer(d18:1/26:0)
NeuAcalpha2-6Galbeta1-3GalNAcbeta1-3Galalpha1-4Galbeta1-4Glcbeta-Cer(d18:1/22:0)
1alpha-hydroxy-23-[3-(1-hydroxy-1-methylethyl)phenyl]-22,22,23,23-tetradehydro-24,25,26,27-tetranorvitamin D3 /1alpha-hydroxy-23-[3-(1-hydroxy-1-methylethyl)phenyl]-22,22,23,23-tetradehydro-24,25,26,27-tetranorcholecalciferol
NeuGcalpha2-8NeuGcalpha2-3Galbeta1-3GalNAcbeta1-3Galalpha1-4Galbeta1-4Glcbeta-Cer(d18:1/16:0)
PS(P-18:0/12:0)
18:1 Cholesteryl ester (d5)
(D)
786-O
(E)
Caki-1-sh-NC
Caki-1-sh-MFN2-1
Caki-1-sh-MFN2-2
ORO
100 μm
Caki-1
IOD of ORO
sh-NC
sh-MFN2-1
sh-MFN2-2
(F)
786-O-sh-NC
786-O-sh-MFN2-1
786-O-sh-MFN2-2
786-O

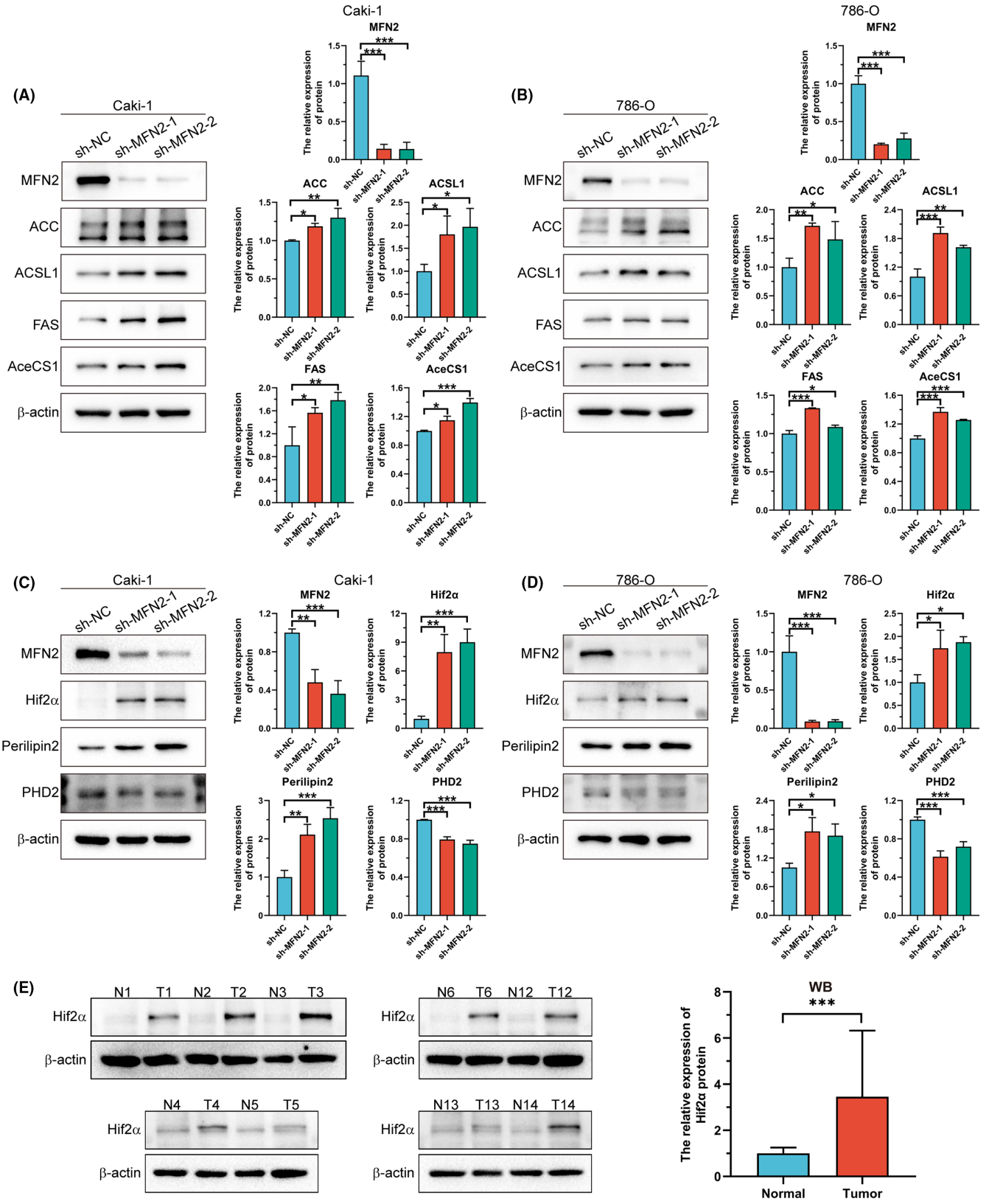

FIGURE 7 Suppressing the expression of MFN2 led to changes of the expression levels of proteins involved in lipid metabolism in clear cell renal cell carcinoma (ccRCC) cells. (A–D) Representative images of Western blot (WB) and plots showing relative levels of proteins involved in lipid metabolism such as ACC, ACSL1AS, AceCS1 (A, B), Hif2α, Perilipin2, and PHD2 (C, D) in addition to MFN2 in Caki-1 (A) and 786-O (B) cells transfected with sh-MFN2-1 and sh-MFN2-2 or a sh-NC virus. (E) Representative images and a quantitative plot showing the differences of Hif2α protein levels between tumor tissues and adjacent normal tissues from ccRCC patients enrolled in our hospital. The first six pairs of tissues are identical with those described in Figure 2D. $^{*}p<0.05$, $^{**}p<0.01$, $^{***}p<0.001$.

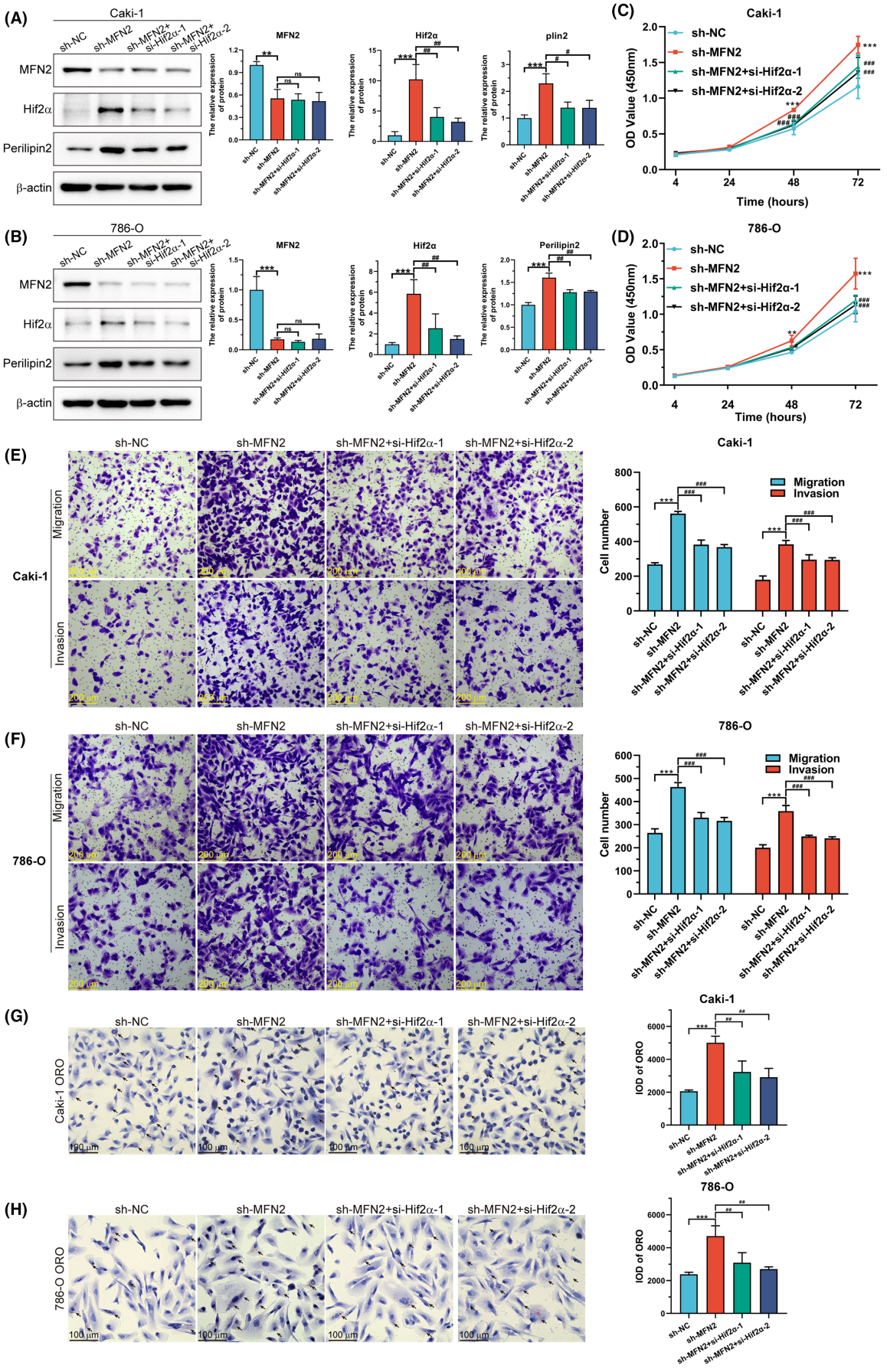

FIGURE 8 Legend on next page

FIGURE 8 MFN2 suppressed the progression of clear cell renal cell carcinoma (ccRCC) and the accumulation of lipid droplets through Hif2α. (A, B) Representative images of Western blot (WB) and plots showing relative levels of MFN2, Hif2α, and Perilipin2 proteins in Caki-1 (A) and 786-O (B) cells transfected with a sh-NC virus or the mixture of sh-MFN2-1 and sh-MFN2-2 with or without two Hif2α-specific siRNA (si-Hif2α-1 and si-Hif2α-2). (C, D) Plots showing the growth curves based on CCK-8 assays in Caki-1 (C) and 786-O cells (D) transfected with a sh-NC virus or the mixture of sh-MFN2-1 and sh-MFN2-2 with or without si-Hif2α-1 and si-Hif2α-2. (E, F) Representative images (left) and statistical analysis (right) showing the migration and invasion abilities of Caki-1 (E) and 786-O cells (F) transfected with a sh-NC virus or the mixture of sh-MFN2-1 and sh-MFN2-2 with or without si-Hif2α-1 and si-Hif2α-2. (G, H) Representative images of oil red O staining and quantitative plots of IOD in Caki-1 (G) and 786-O cells (H) transfected with a sh-NC virus or the mixture of sh-MFN2-1 and sh-MFN2-2 with or without si-Hif2α-1 and si-Hif2α-2. $^{**}p < 0.01$, $^{***}p < 0.001$, versus with sh-NC. $^{\#\#}p < 0.01$, $^{\#\#\#}p < 0.001$, versus with sh-MFN2.

Hif2α is a key therapeutic target for ccRCC, and upregulating Hifs target genes promotes cellular accumulation of lipid droplets.[33] We examined the expression levels of Hif2α protein and found that levels of Hif2α protein were significantly increased in cells whose MFN2 expression was suppressed (Figure 7C,D). Correspondingly, the levels of Hif2α protein in tumor tissues were significantly higher than those in adjacent normal tissues from ccRCC patients enrolled in our hospital (Figure 7E).

Prolyl hydroxylase domain 2 (PHD2) is one of the proline hydroxylases which catalyzes the oxygen-dependent hydroxylation of Hif2α-specific proline residues, leading to binding to pVHL, ubiquitination, and subsequent proteasomal degradation of Hif2α.[34,35] We found that the expression levels of PHD2 were significantly decreased in cells with MFN2 suppressed (Figure 7C,D). These results suggest that MFN2 may sustain the PHD2 levels to promote the degradation of Hif2α protein and accumulation of lipid droplets in ccRCC cells.

3.8 | MFN2 suppressed the progression of ccRCC and the accumulation of lipid droplets through Hif2α

In order to determine the potential role of Hif2α in cells whose expression levels of MFN2 were suppressed, we knocked down the expression of HIF2α with two different kinds of siRNA in MFN2-knockdown cells, which led to the decline of PLIN2 expression (Figure 8A,B). To further confirm this observation, we performed CCK-8 assays, transwell assays, and oil red O staining using MFN2 knockdown cells transfected with siHIF2α and found that the increased proliferation rates, migration and invasion abilities, and accumulation of lipid droplets of these cells caused by MFN2 suppression were reversed when the expression levels of HIF2α were suppressed (Figure 8C–H). These results suggest that MFN2 may suppress the progression of ccRCC carcinoma and the accumulation of lipid droplets through Hif2α in ccRCC cells.

4 | DISCUSSION

As the most dominant form of renal cell carcinomas, ccRCC is characterized by the presence of so-called clear cells, which look like clear soap bubbles under a microscope, because the accumulated lipid droplets in those cells are dissolved by alcohol during the process of tissue sections. The accumulation of lipid droplets in those cells could be caused by either increased lipid synthesis, or reduced lipid degradation, or both. Consistent with another study,[14] we identified MFN2 as the only mitochondrial gene with favorable prognosis which was significantly decreased in ccRCC tissues by bioinformatics analysis and confirmed MFN2 as a tumor suppressor with both cell culture and xenograft models. Lipid metabolite analyses revealed that MFN2 suppressed the accumulation of lipid droplets. Therefore, MFN2 may suppress ccRCC tumorigenesis by reducing the accumulation of lipid droplets.

Currently, multiple studies have shown that mitochondrial dynamics are associated with the initiation and development of cancer in general.[36] Mitochondrion-associated MFN2 is a key protein facilitating mitochondrial fusion.[11] Specifically, MFN2 has been reported to play tumor-suppressive roles in multiple types of cancers, for example, liver cancer,[37] breast cancer,[38] lung cancer,[39] cervical cancer,[40] and pancreatic cancer.[17] Recently, it has also been discovered that MFN2 may serve as a potential prognostic biomarker and therapeutic target for ccRCC.[18] However, the mechanisms by which MFN2 suppresses tumorigenesis are numerous and inconclusive.

Our results indicated that reducing the expression of MFN2 in ccRCC cells led to significant increases in levels of proteins promoting lipogenesis and the synthesis of fatty acids and lipids[27–31] and levels of perilipin2 protein, an outer shell protein surrounding lipid droplets that protects lipid droplets from being degraded through lipophagy, the autophagic degradation of lipid droplets.[32]

Suppressing the expression of MFN2 led to elevation in levels of AceCS1, ACSL1, ACC, and FAS, suggesting an enhancement of lipogenesis and accumulation of lipid droplets. There are reports showing the impact of lipogenesis on the expression of MFN2 and the associated mitochondrial dynamics,[41] while few reports show how MFN2 regulates levels of proteins related to lipogenesis. Von Hippel–Lindau protein (VHL) mutation is a common genetic feature in ccRCC.[42] VHL serves as a substrate recognition component for E3 ligase complex and participates in ubiquitination degradation of Hif2α.[43] VHL mutations lead to abnormal accumulation of the Hif2α protein, an oncogenic protein in ccRCC.[44] Hif2α upregulates CD36 to promote lipid metabolism and reshape the malignant phenotype of ccRCC.[45] Eliminating Hif2α expression can inhibit tumor formation in ccRCC cells lacking VHL.[46] Under normoxic conditions, Hif2α can be hydroxylated by PHD2, followed by its binding to VHL, leading to its degradation.[34,35] Here, we found that silencing the expression of MFN2 in ccRCC

cells suppressed the expression of PHD2 and promoted the expression of Hif2α. Another report showed that Hif2α promotes lipid storage and cell viability by upregulating PLIN2 in ccRCC.[33] Further suppression of Hif2α in MFN2-knockdown cells led to a reduction in expression levels of PLIN2 and a suppression of cell proliferation, migration, and invasion and accumulation of lipid droplets. Therefore, MFN2 reduced the degradation of Hif2α and inhibited lipogenesis.

The accumulation of lipid droplets in cells could be a balance between synthesis and degradation.[26] Our previous report confirmed that enhancing MAP1S-mediated autophagy causes decreases, while suppressing MAP1S-mediated autophagy causes increases in levels of perilipin2 protein and the amount of lipid droplets.[47] MFN2 and its mediated mitochondrial fusion have been shown to promote autophagy.[48] Therefore, MFN2 may suppress the accumulation of lipid droplets by promoting lipophagy. AceCS1,[49] ACSL1,[50] and ACC[51] all promote autophagy so that MFN2 will suppress the levels of those proteins to inhibit autophagy. Thus, the accumulation of lipid droplets resulting from MFN2 suppression is impossible to be caused by the elevation in levels of those proteins because of their enhancement of lipophagy. Both Hif2α and FAS proteins have been reported to be degraded through autophagy[52,53]; thus, MFN2 may enhance the degradation of Hif2α and FAS so that MFN2 suppression leads to the accumulation of Hif2α and FAS to promote lipogenesis.

In summary, MFN2 may cause elevation of proteins related to lipogenesis in autophagy-independent and -dependent ways to enhance synthesis of lipid droplets and/or suppress lipophagy to degrade lipid droplets, leading to accumulation of lipid droplets and progression of ccRCC.

AUTHOR CONTRIBUTIONS

Zhiduan Cai: Conceptualization; data curation; formal analysis; funding acquisition; investigation; methodology; project administration; resources; validation; writing – original draft. **Wenjun Luo:** Conceptualization; data curation; formal analysis; investigation; methodology; validation; writing – original draft. **Haoran Wang:** Data curation; formal analysis; investigation; methodology. **Rui Zhu:** Data curation; formal analysis; investigation; methodology. **Yaoji Yuan:** Data curation; formal analysis; investigation; methodology. **Xiangyu Zhan:** Data curation; formal analysis; investigation; methodology; software; validation; visualization. **Mengyuan Xie:** Data curation; formal analysis; investigation; methodology. **Haoquan Zhuang:** Data curation; formal analysis; investigation; methodology. **Haoyu Chen:** Data curation; formal analysis; investigation; methodology. **Yuyu Xu:** Data curation; formal analysis; investigation; methodology. **Xiezhao Li:** Data curation; formal analysis; investigation; methodology; supervision; validation. **Leyuan Liu:** Conceptualization; data curation; formal analysis; investigation; methodology; project administration; supervision; validation; writing – review and editing. **Guibin Xu:** Conceptualization; data curation; formal analysis; funding acquisition; investigation; methodology; project administration; supervision; validation; writing – review and editing.

ACKNOWLEDGMENTS

We thank all those who helped us with this study.

FUNDING INFORMATION

This work was supported by the National Natural Science Foundation of China (81974392, 82103359), the Key Laboratory of Guangdong Higher Education Institutes (2021KSYS009), the Guangzhou Key Laboratory of Biological Targeting Diagnosis and Therapy (202201020379), the Characteristic Technology Project of Guangzhou Municipal Health Commission (2023C-TS50), the Key Clinical Specialty Project of Guangzhou Medical University (2020), the Key Clinical Specialty Project of Guangdong Province (2022), and the Guangzhou Municipal Science and Technology Project (2024A03J0074).

CONFLICT OF INTEREST STATEMENT

The authors have no conflict of interest.

ETHICS STATEMENT

Approval of the research protocol by an Institutional Reviewer Board: The Ethics Committee of the Fifth Affiliated Hospital of Guangzhou Medical University.

Informed Consent: Informed consent was obtained from the subject(s) and/or guardian(s).

Registry and the Registration No. of the study/trial: N/A.

Animal Studies: Animal procedures involved in this study complied with the Guide for the Care and Use of Laboratory Animals and have been approved by Guangdong Huawei Detection Co., Ltd.'s Experimental Animal Ethics Committee (No. 202208009).

ORCID

Leyuan Liu https://orcid.org/0000-0003-2151-8960
Guibin Xu https://orcid.org/0000-0001-5920-1243

REFERENCES

1. Siegel RL, Miller KD, Wagle NS, Jemal A. Cancer statistics, 2023. *CA Cancer J Clin*. 2023;73(1):17-48.
2. Yang J, Wang K, Yang Z. Treatment strategies for clear cell renal cell carcinoma: past, present and future. *Front Oncol*. 2023;13:1133832.
3. Wettersten HI, Aboud OA, Lara PN, Weiss RH. Metabolic reprogramming in clear cell renal cell carcinoma. *Nat Rev Nephrol*. 2017;13(7):410-419.
4. Saito K, Arai E, Maekawa K, et al. Lipidomic signatures and associated transcriptomic profiles of clear cell renal cell carcinoma. *Sci Rep*. 2016;6:28932.
5. Adebayo M, Singh S, Singh AP, Dasgupta SA-O. Mitochondrial fusion and fission: The fine-tune balance for cellular homeostasis. *FASEB J*. 2021;35:e21620.
6. Ma Y, Wang L, Jia R. The role of mitochondrial dynamics in human cancers. *Am J Cancer Res*. 2020;10(5):1278-1293.
7. Benador IY, Veliova M, Liesa M, Shirihai OS. Mitochondria bound to lipid droplets: Where mitochondrial dynamics regulate lipid storage and utilization. *Cell Metab*. 2019;29:827-835.
8. Bao D, Zhao J, Zhou X, et al. Mitochondrial fission-induced mtDNA stress promotes tumor-associated macrophage infiltration and HCC progression. *Oncogene*. 2019;38:5007-5020.

9. Sun X, Cao H, Zhan L, et al. Mitochondrial fission promotes cell migration by Ca(2+)/CaMKII/ERK/FAK pathway in hepatocellular carcinoma. *Liver Int*. 2018;38:1263-1272.
10. Han YA-O, Kim B, Cho U, et al. Mitochondrial fission causes cisplatin resistance under hypoxic conditions via ROS in ovarian cancer cells. *Oncogene*. 2019;38:7089-7105.
11. Chen KH, Guo X, Ma D, et al. Dysregulation of HSG triggers vascular proliferative disorders. *Nat Cell Biol*. 2004;6:872-883.
12. Chung KA-O, Hsu CA-O, Fan LC, et al. Mitofusins regulate lipid metabolism to mediate the development of lung fibrosis. *Nat Commun*. 2019;10:3390.
13. Boutant M, Kulkarni SS, Joffraud M, et al. Mfn2 is critical for brown adipose tissue thermogenic function. *EMBO J*. 2017;36:1543-1558.
14. Luo L, Wei D, Pan Y, et al. MFN2 suppresses clear cell renal cell carcinoma progression by modulating mitochondria-dependent dephosphorylation of EGFR. *Cancer Commun (Lond)*. 2023;43:808-833.
15. Cai Z, Luo W, Zhuang H, et al. Dual-layer drug release system based on ureteral stents inhibits the formation of ureteral stricture. *Chem Eng J*. 2023;471:144596.
16. Yuan Y, Li X, Xu Y, et al. Mitochondrial E3 ubiquitin ligase 1 promotes autophagy flux to suppress the development of clear cell renal cell carcinomas. *Cancer Sci*. 2019;110:3533-3542.
17. Lin Z, Lin X, Chen J, Huang G, Chen T, Zheng L. Mitofusin-2 is a novel anti-angiogenic factor in pancreatic cancer. *J Gastrointest Oncol*. 2021;12:484-495.
18. Cheng L, Wang Z, Nie L, et al. Comprehensive analysis of MFN2 as a prognostic biomarker associated with immune cell infiltration in renal clear cell carcinoma. *Int Immunopharmacol*. 2022;111:109169.
19. Rojo M, Legros F, Chateau D, Lombès A. Membrane topology and mitochondrial targeting of mitofusins, ubiquitous mammalian homologs of the transmembrane GTPase Fzo. *J Cell Sci*. 2002;115:1663-1674.
20. Scholzen T, Gerdes J. The Ki-67 protein: from the known and the unknown. *J Cell Physiol*. 2000;182:311-322.
21. Strzalka W, Ziemienowicz A. Proliferating cell nuclear antigen (PCNA): a key factor in DNA replication and cell cycle regulation. *Ann Bot*. 2011;107:1127-1140.
22. Tan SK, Hougen HA-O, Merchan JR, Gonzalgo ML, Welford SA-O. Fatty acid metabolism reprogramming in ccRCC: mechanisms and potential targets. *Nat Rev Urol*. 2023;20:48-60.
23. Ackerman D, Tumanov S, Qiu B, et al. Triglycerides promote lipid homeostasis during hypoxic stress by balancing fatty acid saturation. *Cell Rep*. 2018;24:2596-2605.e5.
24. Simha V. Management of hypertriglyceridemia. *BMJ*. 2020;371:m3109.
25. Ridgway ND. The role of phosphatidylcholine and choline metabolites to cell proliferation and survival. *Crit Rev Biochem Mol Biol*. 2013;48:20-38.
26. Walther TC, Farese RV Jr. Lipid droplets and cellular lipid metabolism. *Annu Rev Biochem*. 2012;81:687-714.
27. Ikeda Y, Yamamoto J, Okamura M, et al. Transcriptional regulation of the murine acetyl-CoA synthetase 1 gene through multiple clustered binding sites for sterol regulatory element-binding proteins and a single neighboring site for Sp1. *J Biol Chem*. 2001;276:34259-34269.
28. Luong A, Hannah VC, Brown MS, Goldstein JL. Molecular characterization of human acetyl-CoA synthetase, an enzyme regulated by sterol regulatory element-binding proteins. *J Biol Chem*. 2000;275:26458-26466.
29. Mashek DG, Bornfeldt KE, Coleman RA, et al. Revised nomenclature for the mammalian long-chain acyl-CoA synthetase gene family. *J Lipid Res*. 2004;45:1958-1961.
30. Ha J, Daniel S, Broyles SS, Broyles SS, Kim KH. Critical phosphorylation sites for acetyl-CoA carboxylase activity. *J Biol Chem*. 1994;269:22162-22168.
31. Katsurada A, Iritani N, Fukuda H, et al. Effects of nutrients and hormones on transcriptional and post-transcriptional regulation of fatty acid synthase in rat liver. *Eur J Biochem*. 1990;190:427-433.
32. Gao F, Yao Q, Zhu J, et al. A novel HIF2A mutation causes dyslipidemia and promotes hepatic lipid accumulation. *Pharmacol Res*. 2023;194:106851.
33. Qiu B, Ackerman D, Sanchez DJ, et al. HIF2α-dependent lipid storage promotes endoplasmic reticulum homeostasis in clear-cell renal cell carcinoma. *Cancer Discov*. 2015;5:652-667.
34. Jaakkola P, Mole DR, Tian YM, et al. Targeting of HIF-alpha to the von Hippel-Lindau ubiquitylation complex by O2-regulated prolyl hydroxylation. *Science*. 2001;292:468-472.
35. Cockman ME, Masson N, Mole DR, et al. Hypoxia inducible factor-alpha binding and ubiquitylation by the von Hippel-Lindau tumor suppressor protein. *J Biol Chem*. 2000;275:25733-25741.
36. Vyas S, Zaganjor E, Haigis MC. Mitochondria and cancer. *Mol Cell*. 2016;61:667-676.
37. Wang X, Liu Y, Sun J, et al. Mitofusin-2 acts as biomarker for predicting poor prognosis in hepatitis B virus related hepatocellular carcinoma. *Infect Agent Cancer*. 2018;13:36.
38. Li Y, Dong W, Shan X, et al. The anti-tumor effects of Mfn2 in breast cancer are dependent on promoter DNA methylation, the P21(Ras) motif and PKA phosphorylation site. *Oncol Lett*. 2018;15:8011-8018.
39. Xu K, Chen G, Li X, et al. MFN2 suppresses cancer progression through inhibition of mTORC2/Akt signaling. *Sci Rep*. 2017;7:41718.
40. Wang W, Liu X, Guo X, Quan H. Mitofusin-2 triggers cervical carcinoma cell hela apoptosis via mitochondrial pathway in mouse model. *Cell Physiol Biochem*. 2018;46:69-81.
41. Klimova N, Long A, Scafidi S, Kristian T. Interplay between NAD(+) and acetyl-CoA metabolism in ischemia-induced mitochondrial pathophysiology. *Biochim Biophys Acta Mol basis Dis*. 2019;1865:2060-2067.
42. Gossage L, Eisen T, Maher ER. VHL, the story of a tumour suppressor gene. *Nat Rev Cancer*. 2015;15:55-64.
43. Kaelin WG. Von Hippel-Lindau disease. *Handb Clin Neurol*. 2015;132:139-156.
44. Choueiri TA-O, Kaelin WG Jr. Targeting the HIF2-VEGF axis in renal cell carcinoma. *Nat Med*. 2020;26:1519-1530.
45. Liao M, Li Y, Xiao A, et al. HIF-2α-induced upregulation of CD36 promotes the development of ccRCC. *Exp Cell Res*. 2022;421:113389.
46. Cho H, Du X, Rizzi JP, et al. On-target efficacy of a HIF-2α antagonist in preclinical kidney cancer models. *Nature*. 2016;539:107-111.
47. Xu G, Jiang Y, Xiao Y, et al. Fast clearance of lipid droplets through MAP1S-activated autophagy suppresses clear cell renal cell carcinomas and promotes patient survival. *Oncotarget*. 2016;7:6255-6265.
48. Ashraf R, Kumar SA-O. Mfn2-mediated mitochondrial fusion promotes autophagy and suppresses ovarian cancer progression by reducing ROS through AMPK/mTOR/ERK signaling. *Cell Mol Life Sci*. 2022;79:573.
49. Mariño G, Pietrocola F, Eisenberg T, et al. Regulation of autophagy by cytosolic acetyl-coenzyme A. *Mol Cell*. 2014;53:710-725.
50. Grevengoed TJ, Cooper DE, Young PA, Ellis JM, Coleman RA. Loss of long-chain acyl-CoA synthetase isoform 1 impairs cardiac autophagy and mitochondrial structure through mechanistic target of rapamycin complex 1 activation. *FASEB J*. 2015;29:4641-4653.
51. Gross AS, Zimmermann A, Pendl T, et al. Acetyl-CoA carboxylase 1-dependent lipogenesis promotes autophagy downstream of AMPK. *J Biol Chem*. 2019;294:12020-12039.
52. Shpilka T, Welter E, Borovsky N, et al. Fatty acid synthase is preferentially degraded by autophagy upon nitrogen starvation in yeast. *Proc Natl Acad Sci USA*. 2015;112:1434-1439.

53. Liu XD, Yao J, Tripathi DN, et al. Autophagy mediates HIF2α degradation and suppresses renal tumorigenesis. *Oncogene*. 2015;34:2450-2460.

SUPPORTING INFORMATION

Additional supporting information can be found online in the Supporting Information section at the end of this article.

How to cite this article: Cai Z, Luo W, Wang H, et al. MFN2 suppresses the accumulation of lipid droplets and the progression of clear cell renal cell carcinoma. *Cancer Sci*. 2024;115:1791-1807. doi:10.1111/cas.16151